A 3-D Finite Element Model for Gas-Assisted Injection Molding: Simulations and Experiments

G.A.A.V. Haagh,* G.W.M. Peters,† F.N. van de Vosse, and H.E.H. Meijer

Eindhoven University of Technology, Department of Mechanical Engineering
P.O. Box 513, 5600 MB Eindhoven, The Netherlands

(Presented at the 14th Annual Meeting of the Polymer Processing Society, Yokohama, Japan, June 8-12, 1998)

*Present affiliation: Unilever Research Vlaardingen, The Netherlands.
†Author to whom correspondence should be addressed.

A 3-D Finite Element Model for Gas-Assisted Injection Molding: Simulations and Experiments

G.A.A.V. Haagh*, G.W.M. Peters†, F.N. van de Vosse, and H.E.H. Meijer

Eindhoven University of Technology, Department of Mechanical Engineering
P.O. Box 513, 5600 MB Eindhoven, The Netherlands

Abstract

Although gas-assisted injection molding (GAIM) has been practiced in industry for more than a decade, the process is not completely understood, particularly with respect to the gas penetration mechanism. Consequently, mold design and process control are often governed by trial-and-error, and reliable information on the gas distribution and the final product properties can often only be obtained from experiments. To gain a better understanding of the gas-assisted injection molding process, we have developed a computational model for the GAIM process. This model has been set up to deal with (non-isothermal) three-dimensional flow, in order to correctly predict the gas distribution in GAIM products. It employs a pseudo-concentration method, in which the governing equations are solved on a fixed grid that covers the entire mold. Both the air downstream of the polymer front and the gas are represented by a fictitious fluid that does not contribute to the pressure drop in the mold. The model has been validated against both isothermal and non-isothermal gas injection experiments. In contrast to other models that have been reported in the literature, our model yields the gas penetration from the actual process physics (not from a presupposed gas distribution). Consequently, it is able to deal with the 3-D character of the process, as well as with primary (end of gas filling) and secondary (end of packing) gas penetration, including temperature effects and generalized Newtonian viscosity behavior.

*Present affiliation: Unilever Research Vlaardingen, The Netherlands.
†Author to whom correspondence should be addressed.

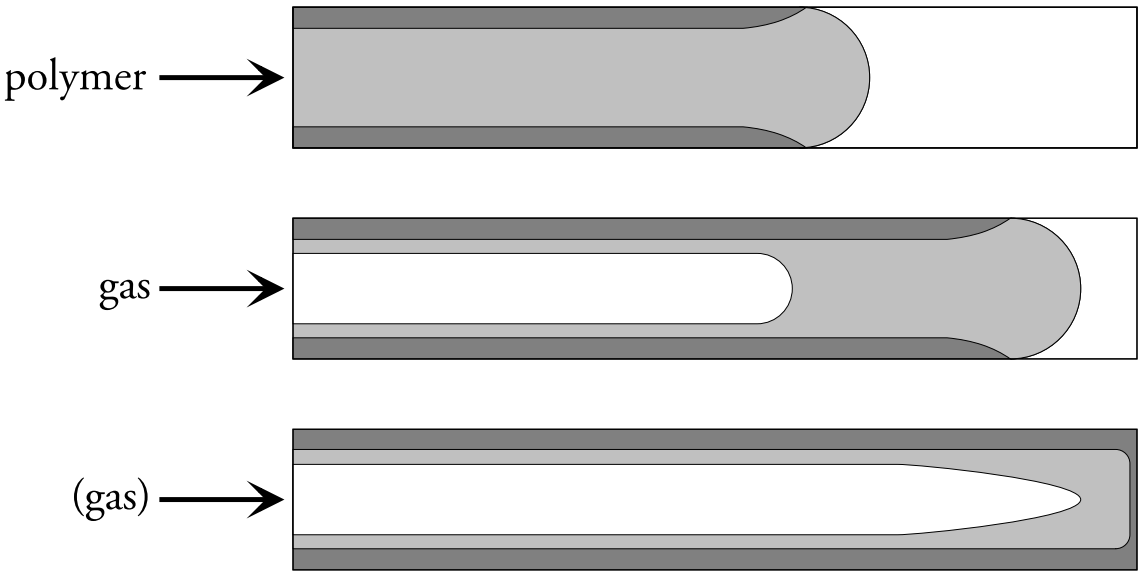

Figure 1: The principle of gas-assisted injection molding: polymer injection (top), gas injection (middle), and packing (bottom). Light grey = polymer melt, dark grey = solidified polymer, white = gas/air.

1 Introduction

In Gas-Assisted Injection Molding (GAIM), gas is injected into a mold that has been partially filled with polymer (see Figure 1). The gas drives the molten polymer core further into the mold, until it is filled completely. The penetrating gas leaves a polymer layer at the mold walls, yielding a product with a polymer skin and a gas core. The gas can either be injected through a needle in the extruder nozzle, or directly into the mold through separate gas injection needles.

After the mold has been entirely filled, gas is used to transmit the packing pressure to the polymer that is being cooled. Any shrinkage of the polymer material near the gas channel is compensated for by an enlargement of the gas core. Once all polymer material has solidified, the gas pressure is released. The product is then further cooled until it has retained sufficient rigidity to be ejected from the mold.

The most important characteristic of GAIM is the fact that the pressure drop in the gas core is negligibly small compared to the pressure drop in an equivalent molten polymer core, because the viscosity of the gas is roughly 10^8 times smaller than that of the polymer. Consequently, the pressure can be considered constant throughout the gas core, and this accounts for most of the advantages of GAIM, such as reduction of clamp force, sink marks and residual stresses, and enhancement of design possibilities.

The injected gas typically penetrates along the path of least flow resistance. This has two consequences: first, any thick-walled part of a mold offers a significantly lower flow resistance than the thin-walled parts that usually make up a major part of the product. The gas is, therefore, inclined to penetrate inside the thick-walled parts, such as ribs and bosses. GAIM product and mold designers should account for this fact, either by properly incorporating ribs to lead the gas flow, or by supplying designated gas-leading channels

[1, 2]. Although the gas will generally penetrate through the thick parts, it may flow into thinner parts as soon as the thick part is completely filled. The second consequence of the gas following the path of least flow resistance, is the inherent instability of the gas front advancement at — apparently symmetric — bifurcations in the mold [3, 4].

Although gas-assisted injection molding has been practiced commercially for more than a decade, the understanding of the characteristics of the process, particularly with respect to the typical flow phenomena, is still lagging behind. These years of practical GAIM experience, mostly gained from trial-and-error, have led to design guidelines for GAIM molds and products, which, however, do not always have an explicit connection to the physics of the process. Consequently, several researchers who have investigated the effect of several parameters on the process and final product, sometimes report contradictory conclusions [5]. A more thorough understanding of the process is expected to establish a clear connection between these process parameters and the process physics, and may hence reveal which parameters are important (and which are not!).

The mechanism of gas penetration is similar to that of a viscous fluid in a tube being displaced by another fluid of lower viscosity, which has been studied for a long time [6–10]. It has been shown that part of the initially present, more viscous fluid remains sticking to the tube wall, and that this fraction is determined by the Capillary number, given by:

$$Ca = \frac{\eta U}{\gamma}. \tag{1}$$

Poslinski *et al.* [11] were among the first to connect this research to gas-assisted injection molding. In order to decouple the thermal and the viscous effects on gas penetration, they performed both isothermal gas injection experiments and an isothermal analysis of the problem. From their dimensional analysis, they concluded that the inertial and gravity effects can be neglected, leaving the Capillary number as the sole factor characterizing the flow.

Their experiments on primary gas penetration in a Newtonian liquid show that the *residual wall thickness* ε, which is defined as the ratio of the residual skin layer of liquid and the tube radius, approaches a value of 0.35 — corresponding to a cross-sectional residual liquid fraction $\phi = 0.58$ — for sufficiently large Capillary numbers ($Ca > 10^2$). As Ca is at least of order 10^3 for the gas injection stage of GAIM, they also neglected interfacial tension effects. From finite element computations, they conclude that ε decreases with increasing power-law exponent for generalized Newtonian fluids (see Figure 2).

The main contributions of Poslinski and co-workers are summarized in the following conclusions:

- The residual polymer wall thickness in GAIM is determined by two phenomena: the penetration of a gas into a viscous liquid, and the growth of a solid layer.
- As the solid layer growth *during* the primary gas injection stage is negligibly small, the contribution of thermal and viscous effects to the residual wall thickness can be decoupled; the final residual wall thickness is the sum of the solid layer thickness at the beginning of gas injection and the liquid polymer layer left behind by the penetrating gas.

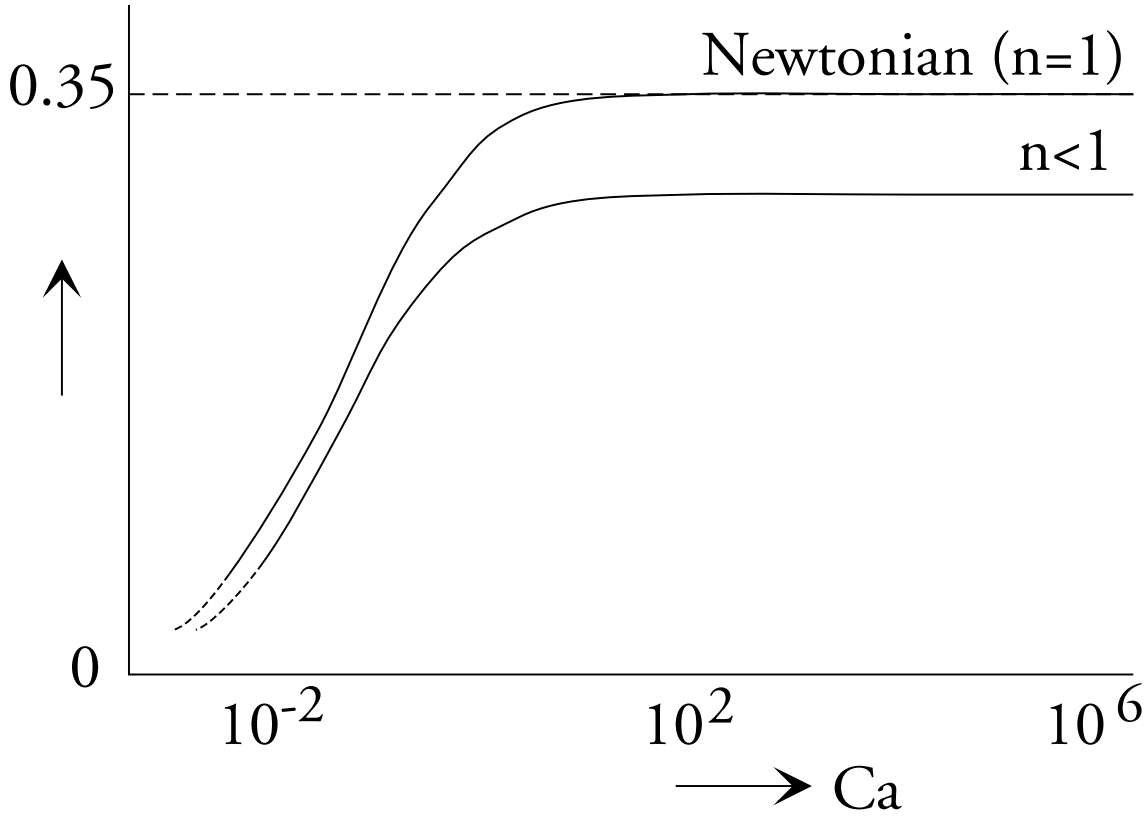

Figure 2: Residual wall thickness as a function of the Capillary number for Newtonian and power-law fluids ($\eta = \eta_0 \dot{\gamma}^{n-1}$). (After Poslinski *et al.* [11].)

- For Newtonian fluids in isothermal flows, the residual wall thickness is only a function of the Capillary number. Non-uniformity of the viscosity, either caused by temperature or shear rate gradients (in the case of non-Newtonian fluids) further affects the residual wall thickness.

Objective

To predict the gas distribution in a product and the resulting product properties, numerical simulations of GAIM can be a powerful tool. Moreover, such simulations may help to increase the understanding of process features and thereby contribute to molding experience. We have therefore developed a computational model for GAIM simulations. It is based on the physics of the process, rather than on a sheer description of the phenomena that are observed. Consequently, this model employs a three-dimensional approach, as gas injection is governed by three-dimensional phenomena. The model has proven to at least qualitatively predict some phenomena that are characteristic for the gas-assisted injection molding process [12–14]. The objective of this paper is to validate this simulation program experimentally, by focusing on the prediction of the gas distribution (usually expressed in terms of residual wall thickness). The numerical results will be compared with experimental results for relatively simple, but yet characteristic, gas injection conditions.

First, the description of the computational model and its numerical implementation will be given, and the experimental set-up will be presented. Subsequently, the simulation results will be compared with experimental data, from which we will eventually draw conclusions with respect to the validity and applicability of the model.

2 Governing Equations

Our model for three-dimensional gas-assisted injection molding simulations is based on a pseudo-concentration method of Thompson [15], which is related to the Volume of Fluid (VOF) method [16]. With this method, the flow problem is solved on a fixed grid that covers the entire mold, so that elaborate three-dimensional remeshing can be avoided. A fictitious fluid is introduced to represent both the air downstream of the polymer flow front and the injected gas. The main property of this fictitious fluid is that its contribution to the pressure build-up in the mold during filling is negligible. Therefore, its viscosity is set to a value at least 10^3 times smaller than the viscosity of the filling fluid. However, the viscosity of the fictitious fluid exceeds the real value for air by several orders of magnitude in order to keep the Reynolds number small, so that inertia terms do not have to be taken into account and turbulence is avoided. Furthermore, the fictitious fluid is allowed to leave the mold at some specified boundaries.

The essence of the pseudo-concentration model is that the distinction between filling fluid and fictitious fluid is made by labelling fluid particles with a material label c (being the pseudo-concentration), which is given the value $c = 1$ for the filling fluid, and $c = 0$ for the fictitious fluid. Near the flow front, c is a continuous function between 1 and 0; the flow front itself is determined by the iso-value line for $c = 0.5$. This interface is kept track of by convecting the material labels with the fluid velocity.

Table 1: Process variables expressed as products of dimensionless variables (marked with an asterisk: *) and characteristic values. (The rate-of-deformation tensor $\mathbf{D}$ has been scaled with the largest components of $\nabla\mathbf{u}$ for $\varepsilon \leq 1$, which are $\frac{\partial u}{\partial y}$ and $\frac{\partial u}{\partial z}$.)

$x = x^* L$	$y = y^* H = y^* \varepsilon L$	$z = z^* H = z^* \varepsilon L$
$u = u^* U$	$v = v^* V = v^* \varepsilon U$	$w = w^* V = w^* \varepsilon U$
$\mathbf{D} = \mathbf{D}^* \frac{U}{H}$	$\varepsilon = \frac{H}{L}$	$p = p^* p_{ref}$
$t = t^* \tau$	$T = T^* (\Delta T)_0$	$\mathbf{g} = \mathbf{g}^* g_0$
$\eta = \eta^* \eta_0$	$\rho = \rho^* \rho_0$	$c_p = c_p^* c_{p0}$
$\lambda = \lambda^* \lambda_0$	$\alpha = \alpha^* \alpha_0$	

The conservation equations for mass, momentum, and internal energy read:

$$\frac{\partial \rho}{\partial t} + (\nabla \cdot \rho \mathbf{u}) = 0 \tag{2}$$

$$\rho \frac{\partial \mathbf{u}}{\partial t} + \rho \mathbf{u} \cdot \nabla \mathbf{u} = \nabla \cdot \sigma + \rho \mathbf{g} \tag{3}$$

$$\rho \dot{e} = \sigma : \mathbf{D} - \nabla \cdot \mathbf{h} + \rho r + \rho h_r R_c. \tag{4}$$

Formally, the conservation of moment of momentum, which requires that the stress tensor is symmetric, is added to this set of equations. Moreover, the use of a pseudo-concentration method demands for an equation for passive scalar convection ('conservation of identity'):

$$\dot{c} = 0, \tag{5}$$

which states that each material particle (actually: each infinitesimal material volume element) in the mold is labelled with a value c that does not change.

2.1 Flow problem

In previous publications [12–14], we have shown through a dimensional analysis that the Navier-Stokes equations for both the polymer domain and the air domain in oblong geometries — of which ribs and other gas-leading channels are typical examples — can be reduced to a stationary Stokes equation:

$$\nabla p = \nabla(2\eta \mathbf{D}), \tag{6}$$

assuming the characteristic values for injection molding that are presented in Table 2. The value $\eta_0 = 10^4\,\mathrm{Pa\,s}$ is characteristic for *non-isothermal* flow of polymer melts in injection molding, *i.e.*, when the polymer cooling is taken into account. Furthermore, the solidified polymer is modeled as an extremely viscous fluid: as soon as the polymer solidifies, its viscosity is set to $10^6\,\mathrm{Pa\,s}$, which exceeds the melt viscosity by, approximately, a factor 10^2–10^3.

Usually, polymer flow is assumed to be incompressible. However, we will retain the original continuity equation (2) in order to be able to compute polymer shrinkage. Thus, we consider the polymer density to be a given function of pressure and temperature:

$$\rho = \rho(p, T). \tag{7}$$

Table 2: Characteristic values of the process variables for thermoplastic injection molding.

variable	unit	characteristic value	
		polymer	air
ρ_0	$\mathrm{kg\,m^{-3}}$	10^3	1
η_0	Pa s	10^4	10^{-5}
c_{p0}	$\mathrm{J\,kg^{-1}\,K^{-1}}$	10^3	10^3
λ_0	$\mathrm{W\,m^{-1}\,K^{-1}}$	10^{-1}	10^{-2}
α_0	$\mathrm{K^{-1}}$	10^{-5}	10^{-3}
L	m	10^{-1}	
H	m	10^{-2}	
U	$\mathrm{m\,s^{-1}}$	10^{-1}	
g_0	$\mathrm{m\,s^{-2}}$	10	
γ_0	$\mathrm{N\,m^{-1}}$	10^{-2}	
$(\Delta T)_0$	K	10^2	

Neglecting the bulk viscosity [14, 17], the dimensionless conservation equation for mass can be written as:

$$Sr\frac{\partial \rho}{\partial t} + (\nabla \cdot \rho \mathbf{u}) = 0. \tag{8}$$

Boundary conditions

We define a domain Ω covering the mold, with boundaries Γ_e, Γ_w, and Γ_v designating the mold entrance, the mold walls, and the air vents. At the mold entrance, either the injection flow rate or the normal stress (*i.e.*, the injection pressure) is prescribed. Wherever the mold wall is covered with polymer, a no-slip condition is imposed.

As a no-slip boundary condition in the air would prevent the polymer from contacting the mold wall, we have chosen to prescribe a free slip condition downstream of the flow front, thus enabling the contact point to move freely [13]. Hence, the boundary condition along the mold walls is a function of the type of material, which is indicated by the material label c. This has been implemented by using an adjustable Robin boundary condition for the (dimensionless) velocity and stress components $\mathbf{u}_t$ and σ_t in tangential direction:

$$a\mathbf{u}_t + \sigma_t = \mathbf{0} \quad \forall \mathbf{x} \in (\Gamma_w \cup \Gamma_v), \tag{9}$$

in which the dimensionless 'Robin penalty parameter' a is defined as

$$a = a(c) = \begin{cases} \text{large } (\geq 10^4) & \text{if } c \geq 0.5\text{: no slip} \\ 0 & \text{if } c < 0.5\text{: free slip} \end{cases}. \tag{10}$$

The mold walls are impermeable, except at the air vents Γ_v where the air is allowed to leave the mold, yielding the following boundary conditions for the velocity and stress component u_n and σ_n in normal direction:

$$u_n = 0 \quad \forall \mathbf{x} \in \Gamma_w \tag{11a}$$
$$a u_n + \sigma_n = 0 \quad \forall \mathbf{x} \in \Gamma_v, \tag{11b}$$

in which a is again given by equation (10) (provided that 'slip' should be replaced by 'leakage').

Interfacial conditions

From a physical point of view, two more boundary conditions hold for the flow front: immiscibility and conservation of momentum. The immiscibility condition is already implied by the 'conservation of identity' (equation 5). The conservation of momentum at the interface is expressed in dimensionless form as [13]:

$$(\sigma_2 - \sigma_1) \cdot \mathbf{n}_{12} = \mathbf{0}, \tag{12}$$

in which the subscripts $_1$ and $_2$ denote the polymer and the fictitious fluid. This condition already taken care of by the overall conservation of momentum equation, since the material properties are continuous functions of c at the interface. As a result, the phenomena at the flow front have already been taken into account in the proper way.

2.2 Temperature problem

Assuming that neither the thermal radiation r nor the reaction heat h_r plays a role in injection molding of thermoplastics, and applying Fourier's law $\mathbf{h} = -\lambda \nabla T$, equation (4) can be reduced to:

$$\rho \dot{e} = \sigma : \mathbf{D} - \nabla \cdot \mathbf{h}. \tag{13}$$

Substitution the appropriate constitutive equations in equation (13) yields:

$$\rho c_p \dot{T} = 2\eta \mathbf{D} : \mathbf{D} + \nabla \cdot \lambda \nabla T + \alpha T \dot{p}, \tag{14}$$

in which the heat capacity coefficient c_p and the heat conduction coefficient λ are given by:

$$c_p = c_p(p, T) \tag{15}$$
$$\lambda = \lambda(p, T). \tag{16}$$

Introducing the dimensionless variables given in Table 1 into this equation yields the dimensionless temperature equation:

$$\frac{1}{Fo}\rho c_p \frac{\partial T}{\partial t} + \varepsilon Pe \rho c_p \mathbf{u} \cdot \nabla T = 2Br\eta \mathbf{D} : \mathbf{D} + \nabla \cdot \lambda \nabla T + \frac{\varepsilon BrSr}{Gc} \alpha T \frac{\partial p_0}{\partial t} + \frac{\varepsilon Br}{Gc} \alpha T \mathbf{u} \cdot \nabla p_0, \tag{17}$$

from which the asterisk (*) indicating dimensionless variables has been removed for convenience. The dimensionless numbers are defined as:

$$Fo = \frac{\lambda_0 \tau}{\rho_0 c_{p0} H^2} \quad \text{Fourier number} \tag{18a}$$

$$Pe = \frac{\rho_0 c_{p0} U H}{\lambda_0} \quad \text{Péclet number} \tag{18b}$$

$$Br = \frac{\eta_0 U^2}{\lambda_0 (\Delta T)_0} \quad \text{Brinkman number} \tag{18c}$$

$$Sr = \frac{L}{\tau U} \quad \text{Strouhal number} \tag{18d}$$

$$Gc = \frac{1}{\alpha_0 (\Delta T)_0} \quad \text{Gay-Lussac number.} \tag{18e}$$

The characteristic time τ in the temperature equation is typically the time in which either the temperature or the pressure changes in the order of its magnitude. For the injection stage, cooling of (hot) polymer melt contacting a (cold) mold wall is roughly estimated to take about 1 second, so that $\tau = 1\,\mathrm{s}$ for this stage. The packing stage is characterized by a fast increase of the pressure, for which τ is of the order of $0.1\,\mathrm{s}$. The temperature decreases rather slowly in the cooling stage, so τ is estimated to be $10\,\mathrm{s}$.

As for the flow problem, a distinction between the polymer and the air domain has to be made, in order to determine which terms of the temperature equation are important in each domain.

Polymer domain

Determining the dimensionless numbers defined in equation (18) from the characteristic values for the polymer as given in Table 2, and substituting these into the dimensionless temperature equation (17) yields the orders of magnitude of the different terms:

$$\underbrace{\frac{1}{Fo}\rho c_p \frac{\partial T}{\partial t}}_{10^3\tau^{-1}} + \underbrace{\varepsilon Pe \rho c_p \mathbf{u}\cdot\nabla T}_{'small'} =$$

$$\underbrace{2Br\eta\mathbf{D}:\mathbf{D}}_{10} + \underbrace{\nabla\cdot\lambda\nabla T}_{1} + \underbrace{\frac{\varepsilon BrSr}{Gc}\alpha T\frac{\partial p_0}{\partial t}}_{10^{-3}\tau^{-1}} + \underbrace{\frac{\varepsilon Br}{Gc}\alpha T\mathbf{u}\cdot\nabla p_0}_{10^{-3}}. \tag{19}$$

The order of magnitude of the convictive term (the second term on the left hand side) is generally small because of the velocity $\mathbf{u}$ and the temperature gradient ∇T are mostly perpendicular. Moreover, the largest temperature gradient is found near the wall in a temperature boundary layer of a limited thickness $\delta < H$, in which the velocity will be very small. This term is only expected to be significant near sharp geometrical transitions, such as corners and flow contractions.

With the given estimates for the characteristic time for the different molding stages, the last two terms of equation (19) can be neglected for all injection stages, leaving the following temperature problem to be solved for the polymer domain:

$$\frac{1}{Fo}\rho c_p \frac{\partial T}{\partial t} + \varepsilon Pe \rho c_p \mathbf{u}\cdot\nabla T = 2Br\eta\mathbf{D}:\mathbf{D} + \nabla\cdot\lambda\nabla T, \tag{20}$$

which is an ordinary convection-diffusion equation. As a matter of fact, the second (convection) and third (dissipation) term can be neglected as well in the cooling stage, since the velocity is approximately zero for that stage.

Air domain

A similar exercise yields the order of magnitude of the temperature equation terms for the air domain:

$$\underbrace{\frac{1}{Fo}\rho c_p \frac{\partial T}{\partial t}}_{10\tau^{-1}} + \underbrace{\varepsilon Pe \rho c_p \mathbf{u}\cdot\nabla T}_{'small'} = \underbrace{2Br\eta \mathbf{D}:\mathbf{D}}_{10^{-6}} + \underbrace{\nabla\cdot\lambda\nabla T}_{1} + \underbrace{\frac{\varepsilon BrSr}{Gc}\alpha T\frac{\partial p_0}{\partial t}}_{10^{-6}\tau^{-1}} + \underbrace{\frac{\varepsilon Br}{Gc}\alpha T\mathbf{u}\cdot\nabla p_0}_{10^{-6}}. \tag{21}$$

Discarding the irrelevant terms results in:

$$\frac{1}{Fo}\rho c_p \frac{\partial T}{\partial t} + \varepsilon Pe \rho c_p \mathbf{u}\cdot\nabla T = \nabla\cdot\lambda\nabla T, \tag{22}$$

which is identical to the resulting equation for the polymer domain, except for the missing viscous dissipation term. However, this term needs a slight re-examination, since we artificially increased the air viscosity when we introduced the fictitious fluid. Thus, for the fictitious fluid, the Brinkman number is of order 10^{-2}, indicating that the use of a fictitious fluid will hardly affect the temperature solution.

Consequently, applying equation (20) on the entire computational domain would yield a sufficiently accurate temperature solution. However, the viscous dissipation term should be set to zero for the air domain, since the computed velocity field in the fictitious fluid does not represent the actual air velocity distribution.

Initial and boundary conditions

As an initial condition for the temperature problem, a temperature field over the entire domain is imposed:

$$T = T_0(\mathbf{x}) \quad \forall \mathbf{x}\in\Omega, t = 0. \tag{23}$$

At the injection gate Γ_e, the injection temperature is prescribed:

$$T = T_e(t) \quad \forall \mathbf{x}\in\Gamma_e, t > 0. \tag{24}$$

The boundary conditions at the mold walls and air vents can either be a constant temperature (Dirichlet boundary condition):

$$T = T_w(t) \quad \forall \mathbf{x}\in(\Gamma_w\cup\Gamma_v), t > 0, \tag{25}$$

or a prescribed heat flux (Biot or Robin boundary condition):

$$\lambda \frac{\partial T}{\partial \mathbf{n}} = h_w (T - T_w) \quad \forall \mathbf{x} \in (\Gamma_w \cup \Gamma_v), t > 0, \tag{26}$$

in which $\mathbf{n}$ is the normal vector on the mold wall, h_w is the effective heat transfer coefficient from the polymer to the cooling medium, and T_w is the wall temperature.

Since the actual temperatures at the mold wall are rarely known accurately, a complete thermal analysis of the mold (including the cooling channels *etc.*) would yield a more reliable molding simulation. However, such an extension of the analysis is beyond the scope of this paper.

At the air/polymer interface(s), the temperature is continuous. Solving the temperature equation (20) on a fixed grid will inherently satisfy this condition.

2.3 Material label convection problem

The material labels that are used to distinguish polymer from air, are convected through the mold with velocity $\mathbf{u}$, while maintaining their 'identity' according to equation (5). Hence, in a Eulerian coordinate system, a pure (passive scalar) convection equation describes the evolution of the material label distribution; in its dimensionless form, it reads:

$$Sr \frac{\partial c}{\partial t} + \mathbf{u} \cdot \nabla c = 0. \tag{27}$$

Initially, c is set to zero in the entire domain Ω, and only boundary conditions at the flow entrance are needed:

$$c = 0 \quad \forall \mathbf{x} \in \Omega, t = 0 \tag{28a}$$

$$c = 1 \quad \forall \mathbf{x} \in \Gamma_e, 0 < t < t_{gas} \tag{28b}$$

$$c = 0 \quad \forall \mathbf{x} \in \Gamma_e, t \geq t_{gas}, \tag{28c}$$

in which t_{gas} is the time when gas is injected.

The boundary condition for the convection equation can also be the time of entrance (injection time) or one of the entrance coordinates. Equation (27) can then be used to perform particle tracking to visualize the flow [18].

The material properties, as they appear in the Stokes equation, can now be determined locally as a function of the material label. The mold filling problem can thus be simulated by solving equations (6) and (27), and updating the material properties at every time step.

2.4 Numerical methods

The continuity equation (8) and the Stokes equation (6) are solved using a standard Galerkin finite element method. Unlike in the purely incompressible case, the system of element equations for the continuity equation has a non-zero right hand side vector, as it takes into account the local time derivative of the density through a first order approximation in time.

The material parameters are defined as discontinuous functions of the material labels, *e.g.*, for viscosity:

$$\eta = \eta(c) = \begin{cases} \eta_{polymer} & \text{if } c \geq 0.5 \\ \eta_{fictitious} & \text{if } c < 0.5 \end{cases} \tag{29}$$

The temperature and the label convection equations are solved with the finite element method using an Streamline Upwind Petrov-Galerkin scheme. A finite difference θ-method was used for the temporal discretisation. The material labels are rounded off to either unity or zero everywhere, except in the elements containing the flow front, where the original values of the material labels are retained. Hence, oscillations in the material label field are suppressed, and the flow front is tracked more accurately.

The model, as it has been described in the previous sections, has been implemented in the finite element package SEPRAN [19]. A more comprehensive explanation of the numerical methods can be found in references [12–14].

3 Experimental methods and materials

To validate the computational model for gas-assisted injection molding, a number of gas injection experiments were set up. As argued in the introduction, the residual thickness consists of a solidified layer (governed by thermal effects) and a melt layer (governed by viscous behavior). The viscous contribution is investigated separately by performing two types of experiments: isothermal experiments, in which the temperature effects are disregarded; and non-isothermal experiments, in which the thermal conditions are used to affect the viscosity behavior.

Consequently, we built two experimental set-ups for our validation experiments: one for gas injection experiments in a axisymmetric cylinder (in the tradition of Poslinski and co-workers [11]), and another one for gas injection in a plaque with a rib.

3.1 Cylinder set-up

The experimental set-up for gas injection experiments consists of two hollow coaxial cylinders separated by a spiral groove (Figure 3). Initially, the cavity is filled with 4 mm thick tablets of polystyrene to a height that is sufficient to prevent gas breakthrough (usually 70–80% of the cylinder height). Then the cylinder is heated by pumping hot oil through the spiral groove. Cooling the cylinder is done by switching to cold oil. By stacking alternatingly black and yellow polystyrene tablets into the cylinder, the flow patterns can be visualized.

Five type J (iron/constantan) thermocouples are used to monitor the temperature at approximately 3 mm from the inner mold wall. In each experiment, the cylinder is heated long enough for the polystyrene to obtain a constant temperature. Nitrogen gas can be injected through a pressure valve either before cooling (isothermal gas injection) or after allowing for a stagnant polymer layer to develop (non-isothermal gas injection). The gas pressure is in the order of a few bar only, and gas injection may take from a few seconds to a few minutes to fill the entire cylinder. One might object that the pressures used in these experiments are much lower than the gas injection pressures that are common in GAIM

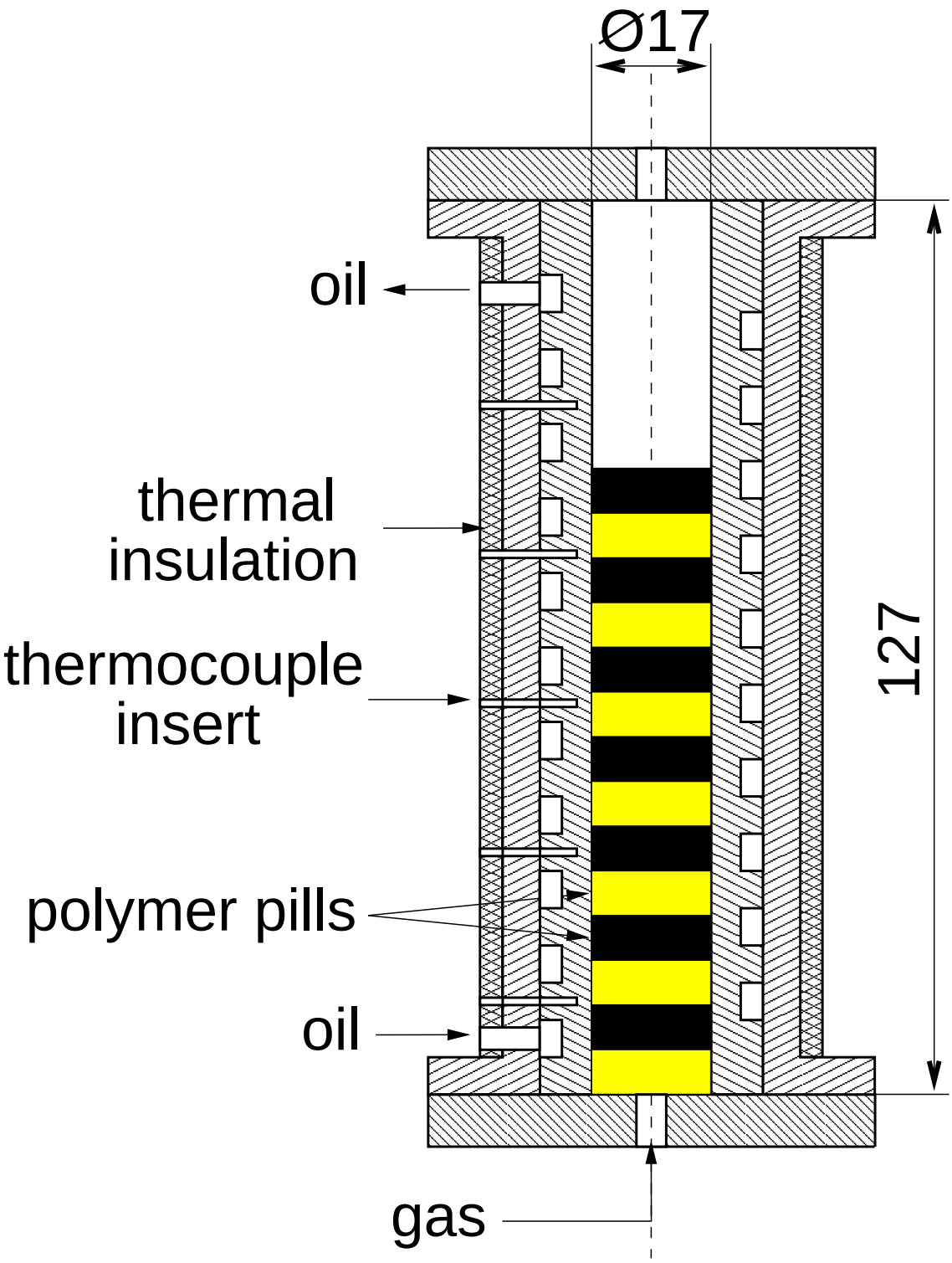

Figure 3: Experimental set-up for GAIM experiments in an axisymmetric cylinder.

practice. However, it was advocated in the introduction that the residual wall thickness is only a function of the viscosity behavior and the Capillary number, and not of the pressure.

After the mold has cooled sufficiently, the sample is pressed out of the cylinder and cut in half. In this way, the gas distribution and melt deformation can be visualized and the residual wall thickness can be measured.

3.2 Plaque-with-rib set-up

The plaque-with-rib set-up, which is depicted in Figure 4(a), represents a commonly used GAIM geometry, as ribs often serve as gas-leading channels. Several rib geometries and their effect on the gas core size have been reviewed in the literature [2, 20], and the effect on product strength and stiffness has been investigated [21]. The rib geometry in our set-up has been designed in accordance with the guidelines given by Rennefeld [2].

The principle of the plaque-with-rib set-up is similar to the cylinder set-up: pre-molded polystyrene inserts (in three parts: plaque, rib foot, and rib) are put inside the mold. The mold is closed and submerged into a hot oil bath, in order to melt the polystyrene inserts. After the mold has attained a homogeneous temperature (which is measured as the oil temperature), gas can be injected. Once the process is completed, the mold is cooled in a cold oil bath (*i.e.*, at room temperature), after which the specimen can be removed from the mold. For non-isothermal experiments, the gas is injected after the mold has been submerged into the cold bath for a specified time. The specimen is cut into slices perpendicular to its length direction, and the residual wall thicknesses are measured.

Although our set-up enables isothermal gas injection experiments, it does lack one particular feature of a real injection molding machine: the polymer melt inside the mold cannot be pressurized before the actual gas injection. It appeared that, as a result of this, the gas did not always penetrate into the molten polystyrene, but often found its way towards the mold walls, along which it escaped to the air vents. In particular, when the mold was submerged into the cold oil bath (for non-isothermal experiments), the polymer shrinkage definitely provided such a 'short circuit' from the injection gate to the air vents. As a consequence, non-isothermal gas injection experiments turned out to be impossible with this set-up, and the gas penetration was hard to control in the isothermal experiments.

3.3 Material properties

The polystyrene used in the experiments is Styron 678E from DOW Chemical. The shear viscosity of this polystyrene is described by a 7-constant Cross model [22]:

$$\eta(p,T,\mathbf{D}) = \frac{\eta_0}{1+\left(\eta_0|II_{2\mathbf{D}}|/\tau^\star\right)^{1-n}}, \tag{30a}$$

in which $II_{2\mathbf{D}}$ is the second invariant of (twice) the rate-of-deformation tensor, and η_0 is the zero shear rate viscosity given by:

$$\eta_0(T) = \eta_0(T^\star)\mathrm{e}^{\frac{-c_1(T-T^\star)}{c_2^\star+T-T^\star}} \tag{30b}$$

$$T^\star = T_0 + s\cdot p \tag{30c}$$

$$c_2^\star = c_2 + s\cdot p. \tag{30d}$$

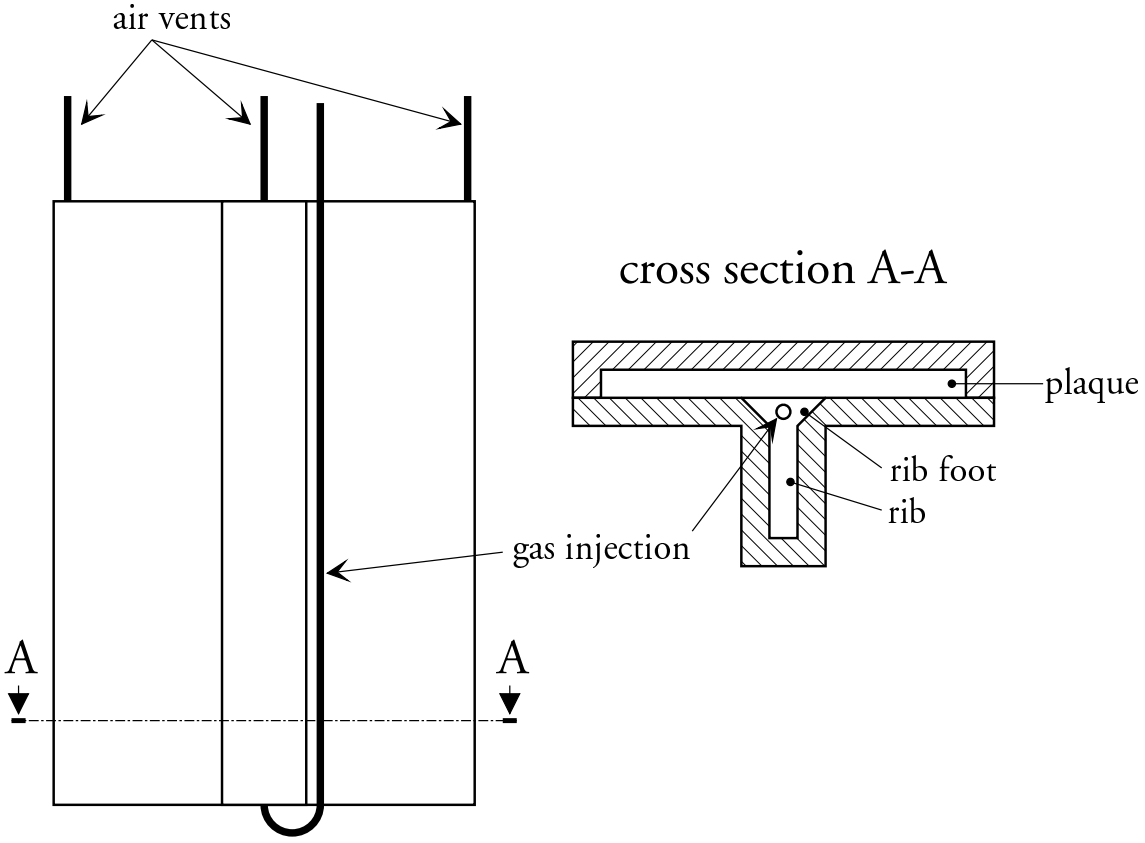

(a) Experimental set-up

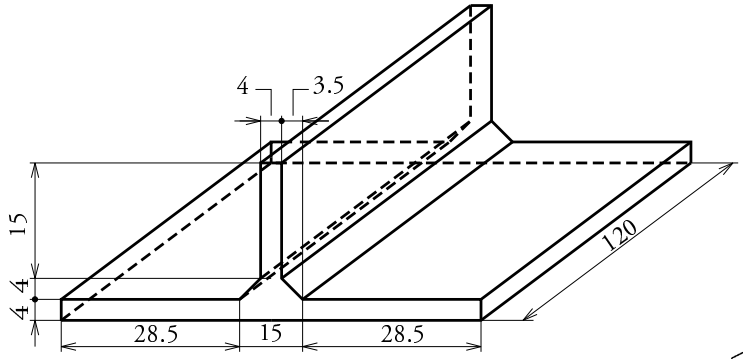

(b) Dimensions.

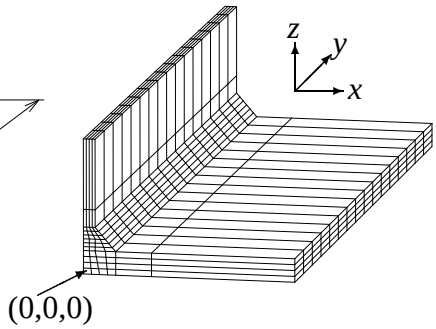

(c) Mesh.

Figure 4: Plaque-with-rib geometry (dimensions in mm). For reasons of symmetry, only one half has to be meshed.

Table 3: Material parameters for polystyrene Styron 678E from DOW Chemical (after [22]).

(a) Viscosity parameters.

n		0.2520
$\tau^\star$	Pa	$3.080 \cdot 10^4$
$\eta_0(T^\star)$	Pa s	$4.76 \cdot 10^{10}$
T_0	K	373
c_1		25.74
c_2	K	61.06
s	$\mathrm{K\,Pa^{-1}}$	$5.1 \cdot 10^{-7}$

(b) Specific volume parameters.

		melt	glass
a_0	$\mathrm{m^3 kg^{-1}}$	$9.72{\cdot}10^{-4}$	$9.72{\cdot}10^{-4}$
a_1	$\mathrm{m^3 kg^{-1} K^{-1}}$	$5.44{\cdot}10^{-7}$	$2.24{\cdot}10^{-7}$
B_0	Pa	$2.53{\cdot}10^{8}$	$3.53{\cdot}10^{8}$
B_1	$\mathrm{K^{-1}}$	$4.08{\cdot}10^{-3}$	$3.00{\cdot}10^{-3}$
T_{g0}	K	373	
s	$\mathrm{K\,Pa^{-1}}$	$5.1{\cdot}10^{-7}$	

(c) Thermal properties.

		melt	glass
λ	$\mathrm{W m^{-1} K^{-1}}$	0.17	0.17
c_p	$\mathrm{J kg^{-1} K^{-1}}$	2289	1785

Table 4: Material parameters for nitrogen gas (at $T = 273\,\mathrm{K}$ and $p = 0\,\mathrm{MPa}$; from [26]).

v	$\mathrm{m^3 kg^{-1}}$	0.8
λ	$\mathrm{W m^{-1} K^{-1}}$	25
c_p	$\mathrm{J kg^{-1} K^{-1}}$	$1.04 \cdot 10^3$

The pvT-behavior of the polystyrene can be described by a so-called double-domain Tait equation [23]:

$$v(p,T) = \begin{cases} (a_{0s} + a_{1s}(T - T_{g0}))\left(1 - 0.0894 \ln\left(1 + \frac{p}{B_s}\right)\right) & \text{if } T \le T_g \\ (a_{0m} + a_{1m}(T - T_{g0}))\left(1 - 0.0894 \ln\left(1 + \frac{p}{B_m}\right)\right) & \text{if } T > T_g \end{cases} \tag{31a}$$

$$T_g = T_{g0} + s \cdot p \tag{31b}$$

$$B_s = B_{0s} e^{-B_{1s}(T-273)} \tag{31c}$$

$$B_m = B_{0m} e^{-B_{1m}(T-273)}. \tag{31d}$$

The parameters for the Cross model and the Tait equation, as well as the thermal properties, are given in Table 3.

The thermal conductivity and thermal capacity are assumed constant for each phase. For the nitrogen gas that is injected, we assume the relevant properties to be constant within the window of processing conditions; these properties are given in Table 4.

Table 5: Experimental conditions for the gas injection experiments in an axisymmetric cylinder.

case	temperature [°C]	pressure [10^5 Pa]	initial filling	t_{delay} [s]
isothermal, Newtonian	171	1.0	67%	–
isothermal, shear-thinning	179	5.8	67%	–
non-isothermal	170	5.8	81%	75

4 Experimental validation

For a comparison of experimental and numerical results, we will focus on the residual wall thickness as the most important quantity. Furthermore, the stacking of alternatingly black and yellow polymer in the cylinder mold (see Figure 3) enables us to visualize the polymer flow patterns through experimental particle tracking, which can be compared directly to the numerical particle tracking results.

4.1 Axisymmetric cylinder

With the axisymmetric cylinder set-up, three different experiments have been carried out under the conditions that are given in Table 5. When gas is injected at an overpressure of 1.0 bar into the cylinder filled with polystyrene that has a uniform temperature of 171°C, the shear rate is low enough for the polymer viscosity to be on the Newtonian plateau (see Section 3.3). Hence, if shrinkage were to be neglected, a residual wall thickness of approximately 36% would be expected. The shrinkage of the polymer will cause this fraction to be somewhat smaller. Isothermal shear-thinning conditions are obtained when the gas is injected at 5.8 bar overpressure into polystyrene of 179°C. According to [11], shear-thinning will cause the residual wall thickness to decrease (see Figure 2). In the non-isothermal experiment, the polymer is cooled for 75 seconds from an initial homogeneous temperature of 170°C before the gas is injected. At that time, the wall temperature has decreased to approximately 150°C, which causes a ten-fold increase in the (zero shear-rate) viscosity near the mold wall compared to the viscosity in the center. Consequently, the residual wall thickness is expected to be larger than in the isothermal cases. The temperatures given in Table 5 are average values over the cylinder length, since both the temperatures at the top and bottom of the cylinder were about 5°C lower than at the central part. Simulations showed that these temperature differences did not have any significant effect on the results.

Five experiments were carried out for each case of experimental conditions. The specimens were cut in half, after which the residual wall thickness was measured with a micrometer at 10 mm intervals along the cylinder length at both sides of the gas core.

The simulation results for the residual wall thickness fraction ε and the filling time are compared with the experimental results in Figures 5 and 6, and in Table 6. Apart from some minor entrance effects, the agreement for the residual wall thicknesses in the isothermal cases is good. Also the filling time is predicted well. The slight deviation of the results for the Newtonian case from the value of $\varepsilon = 0.36$ can be accounted for

Table 6: Experimental and numerical results for gas injection in the cylinder mold. The residual wall thickness is averaged over the domain $30\,\text{mm} \leq z \leq 70\,\text{mm}$, where z is the axial distance from the gas injection point.

case	residual wall thickness [%]		filling time [s]	
	experiment	simulation	experiment	simulation
isothermal, Newtonian	34.6±0.8	33.8	92 ±15	98
isothermal, shear-thinning	31.8±0.9	32.0	3.2± 0.5	4.7
non-isothermal	54.0±1.2	45.8	13.1± 5.1	29

by the shrinkage of the polystyrene. Shear-thinning does indeed cause a slight decrease in the residual wall thickness, which is in accordance with the conclusions of [11]. The filling time for this case is much shorter due to the higher pressure, and some discrepancy between the experimental and the computed value is found.

One can calculate that, for this geometry, the secondary gas penetration due to shrinkage in the packing stage has a marginal effect on the residual wall thickness (see Appendix B).

The difference between experiment and simulation is larger for the non-isothermal case, although the general trend is predicted well (see the solid line in Figure 6(c)). If this discrepancy between measured and computed residual wall thickness were due to a lag between the measured and the actual mold wall temperatures, then Figure 6(c) would suggests that the actual wall temperature should be lower. Simulation shows that a 5°C decrease in wall temperature does indeed yield a larger residual wall thickness, although it covers only half the original gap between numerical and experimental values. Prescribing an actual wall temperature in the simulations that is about 10°C lower than the measured temperature might yield coinciding experimental and numerical results, but such a large temperature difference is very unlikely to occur in the actual experiment. Moreover, the 5°C decrease in wall temperature doubles the calculated filling time, which was already twice as long as the experimental filling time.

Closer examination of the specimens from the non-isothermal experiments revealed that the experimental gas contours sometimes were highly irregular, with polymer indentations protruding into the gas core; this causes the experimental error in the non-isothermal case to be larger than in the isothermal cases (compare the error bars in Figure 6(c) to those in Figures 6(a) and 6(b)). To explain this, we recall that the cylinder had been initially filled with a stack of polystyrene pills. Stacking these pills is believed to give rise to contaminations and small air gaps at the interfaces between these pills. It seems that under high shear deformation such as shown in Figure 5(c), the material (partly) loses its coherence at the interface between two pills. The gas then supposedly breaks through the polymer pill that covers the gas front. Consequently, the number of polymer layers downstream of the gas front decreases, which can be seen in the left half of Figure 5(c): of the original 16 colored layers, only ten are found between the gas core and the top of the specimen. The remaining six layers are visible as alternating light and dark shades of grey at the surface of the gas core. This 'local breakthrough' effect is accompanied by local increases in wall thickness at the transitions between pills, which is shown for an extreme case in Figure 5(d). In this respect, we suggest that the experimental values in

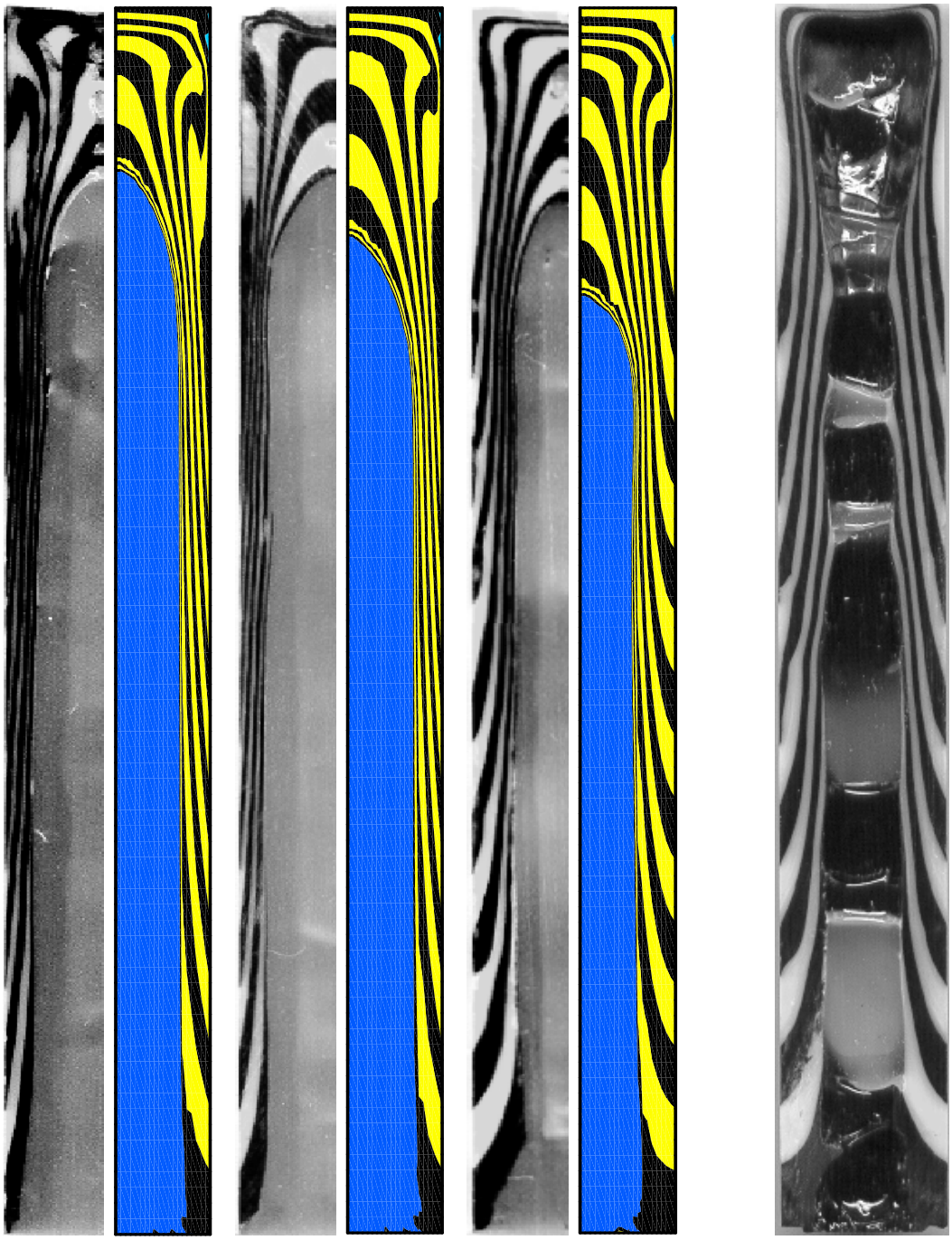

(a) (b) (c) (d)

Figure 5: Comparison of experimental (left) and numerical (right) flow patterns for gas injection into an axisymmetric cylinder; (a): isothermal Newtonian case, (b): isothermal shear-thinning case, (c): non-isothermal case, (d): a specimen exhibiting severe ‘local breakthrough’ of polymer pills (non-isothermal case).

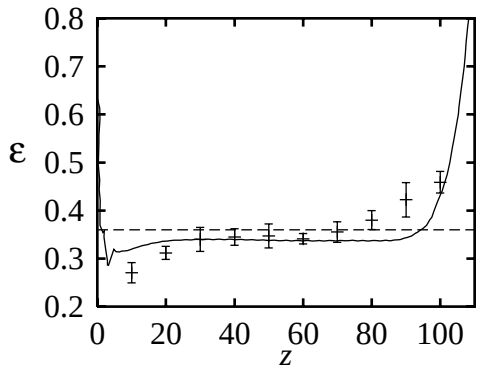

(a) Isothermal, Newtonian.

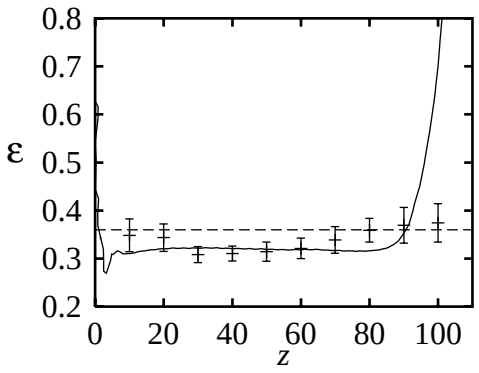

(b) Isothermal, shear-thinning.

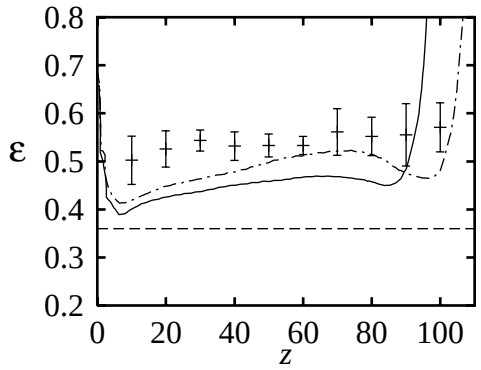

(c) Non-isothermal.

Figure 6: Comparison of experimental and numerical results for gas injection into an axisymmetric cylinder: relative residual wall thickness ε along the axial distance z from the gas injection point (error bars = experimental results; solid line = numerical result; dashed line: Newtonian 36% limit). The dash-dot line in (c) has been obtained by assuming a 5 °C lower wall temperature.

Figure 6(c) be regarded as an 'upper bound' for the residual wall thickness. Apparently, the breakthrough of polymer layers decreases the flow resistance, and hence decreases the experimental filling time, which is less than half the computed filling time. Local breakthrough of polymer layers has also been found in the isothermal experiments, but to a much lesser extent, and usually for $z > 90$ mm, so that the influence on the residual wall thickness is very small.

4.2 Plaque-with-rib

In the plaque-with-rib experiment, nitrogen gas was injected at an overpressure of 3.0 bar into polystyrene having a homogeneous temperature of 180°C. This gas pressure was maintained during the cooling of the mold. Eventually, four specimens were obtained

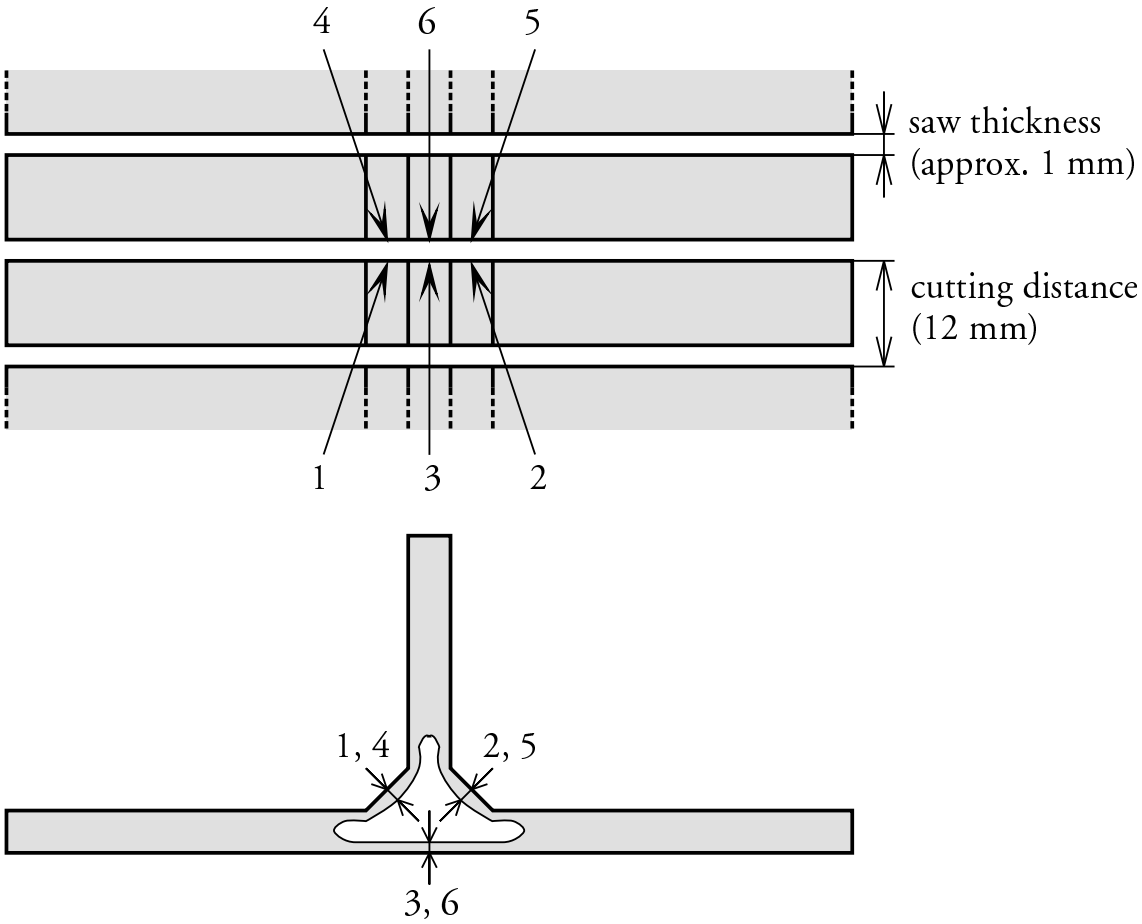

Figure 7: Locations of residual wall thickness measurements for the plaque-with-rib specimens: top view (top) and cross-sectional view (bottom). Note that for every cross section, two rib bottom thicknesses (positions 3 and 6) and four rib flank thicknesses (positions 1, 2, 4, and 5) are measured.

from the isothermal experiments. These specimens were cut into ten slices along the length direction, after which the residual wall thicknesses at the center of the rib bottom and the rib flanks (indicated in Figure 7) were measured with a micrometer. The set-up did not allow the filling times to be measured accurately; roughly, they were of the order of 30 seconds.

The mold geometry and computational mesh for the simulation of this experiment are depicted in Figure 4(b). This mesh is rather coarse as compared to the meshes used in the previous sections. Yet, it consists of 896 brick elements, which yield nearly 30 000 degrees of freedom for the Stokes equations. It took approximately $2\frac{1}{2}$ days of CPU-time to simulate the experiment on a Silicon Graphics workstation with an R10000 processor.

The numerically and experimentally obtained gas core contours for this experiment, as shown in Figures 8 and 9, appear to match well. The numerical results also demonstrate that the contribution of the polymer shrinkage (also called ‘secondary gas penetration’) to the final gas core size proves to be significant: this is indicated by the area between the solid lines and the grey (polymer) area in Figure 8. In Figure 10 and Table 7, the residual

Table 7: Experimental and numerical residual wall thickness for gas injection into the plaque-with-rib mold. The values are averaged over the domain 12 mm $\leq y \leq$ 84 mm, where y is the axial distance from the gas injection point.

position	residual wall thickness [%]	
	experiment	simulation
rib bottom	26.7±0.7	21.0
rib flank	24.3±0.6	23.7

wall thicknesses have been related to the hydraulic radius of the triangle that makes up the rib. The wiggles in the simulation results are due to the coarseness of the mesh. There is a good quantitative agreement between numerical and experimental results. The slight under-prediction of the rib bottom wall thickness may be attributed to the mesh, which is coarser near the rib bottom than near the rib flank (see Figure 4(b)).

4.3 Discussion

Both isothermal and non-isothermal gas injection experiments in a cylinder mold were carried out to validate our model for gas-assisted injection molding. The simulations of the isothermal cases yielded results that agreed well with the experimental results. In particular, the effect of shear-thinning viscosity behavior on the residual wall thickness was predicted correctly. For the non-isothermal experiment a qualitative agreement was found: mold cooling was seen to increase the residual wall thickness, as expected. The quantitative discrepancy between the numerical and experimental results for this case can, to a large extent, be attributed to experimental problems.

The simulation of an isothermal gas injection experiment in a plaque-with-rib mold demonstrates the model's ability to deal with three-dimensional geometries. Moreover, polymer shrinkage was found to have a significant effect on the final size of the gas core. Unfortunately, experimental difficulties related to the unstable nature of gas penetration prohibited reproducible non-isothermal experiments to be executed with the plaque-with-rib set-up. To facilitate such experiments, an injection molding machine with a gas injection unit is required. However, our main conclusions regarding the modeling of GAIM are *not* affected by the absence of a fully three-dimensional, non-isothermal gas injection experiment, since the model does not treat two-dimensional (axisymmetric) gas-assisted injection molding fundamentally different from its three-dimensional counterpart.

This leads us to the three-dimensional nature of the gas penetration phenomenon. The residual wall thickness fraction is obviously the result of a force balance between the gas pressure and the (viscous) stresses in the penetrated liquid. Consider the penetration of an inviscid gas into an axisymmetric cylinder filled with a viscous liquid. For Newtonian liquids, the residual wall thickness fraction is approximately 0.36, irrespective of the liquid viscosity (or, equivalently, irrespective of the gas pressure). If the cylinder is filled with a shear-thinning fluid, the residual wall thickness becomes a function of the power-law exponent, as is shown by the simulation results in Figure 11 and by the observations of Poslinski *et al.* [11].

The residual wall thickness ε cannot be derived from the shear stress distribution far

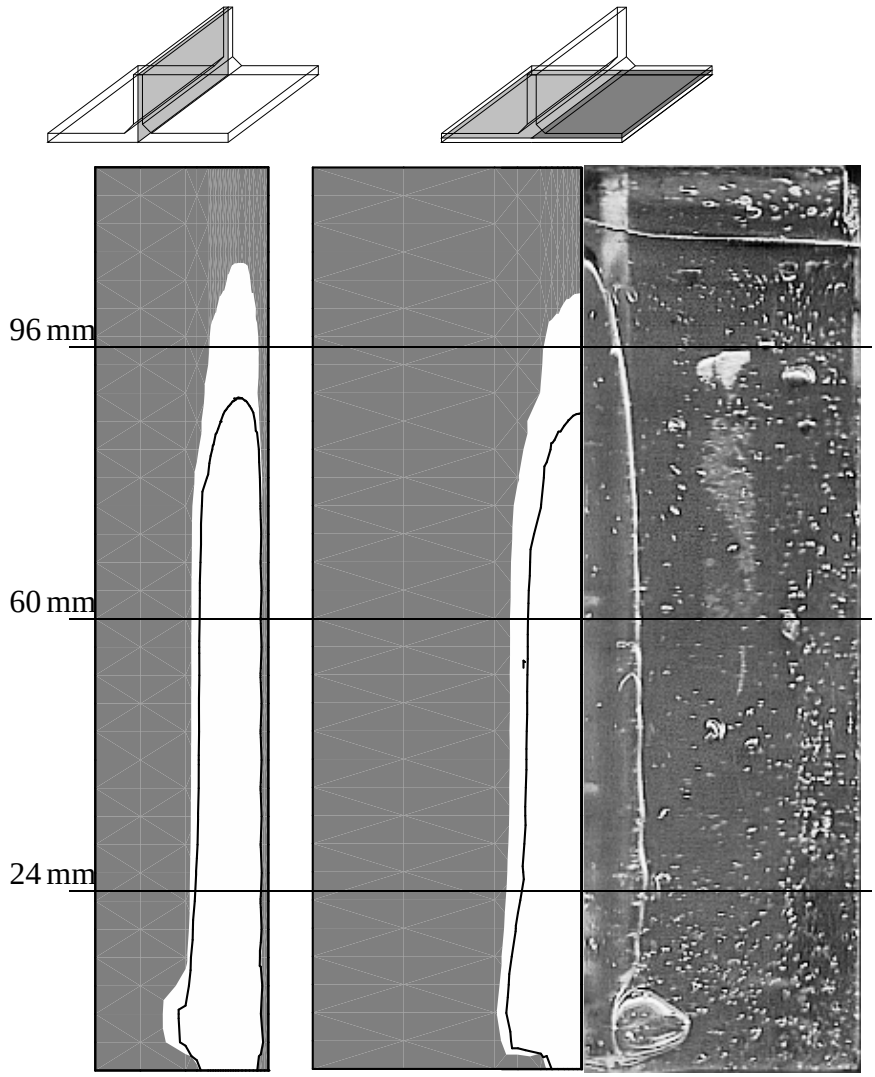

Figure 8: Isothermal gas injection simulation for the plaque-with-rib. (a): Simulation result for cross section $x = 0\,\text{mm}$. (b): Simulation result for cross section $z = 2\,\text{mm}$. (c): Photograph of the bottom ($z = 0\,\text{mm}$) of a transparent specimen (the nearly horizontal line just above the gas bubble contour is a crack). The lines in (a) and (b) depict the gas bubble contours at the end of the filling stage, *i.e.*, before any shrinkage has occurred.

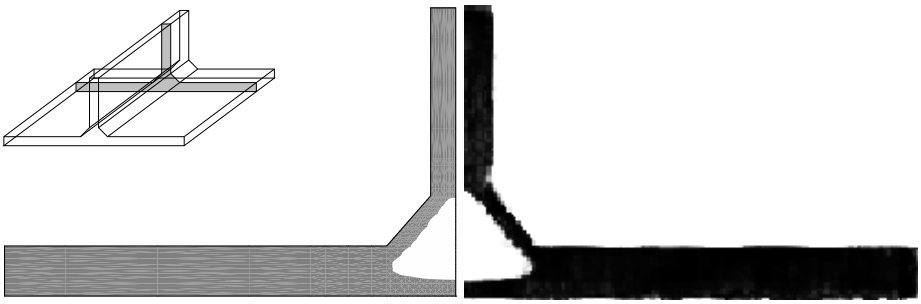

(a) $y = 96\,\text{mm}$

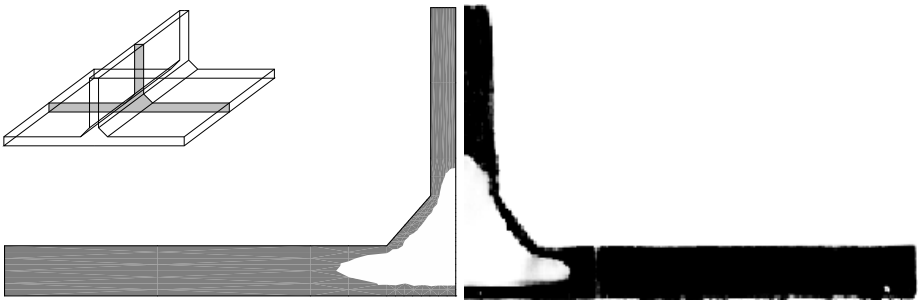

(b) $y = 60\,\text{mm}$

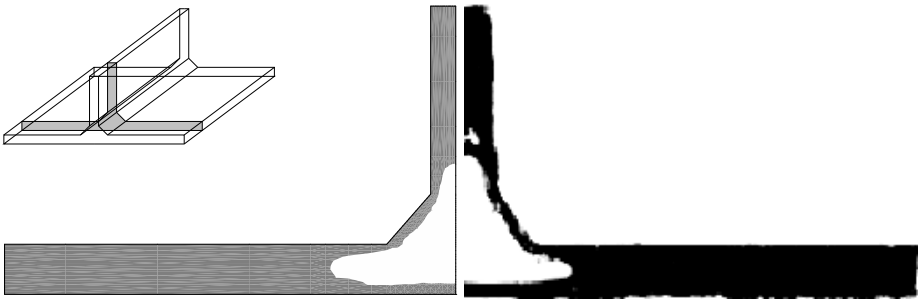

(c) $y = 24\,\text{mm}$

Figure 9: Isothermal gas injection for the plaque-with-rib: comparison of simulation (left) and experimental (right) results at different cross sections perpendicular to the y-direction (corresponding to the horizontal lines in Figure 8).

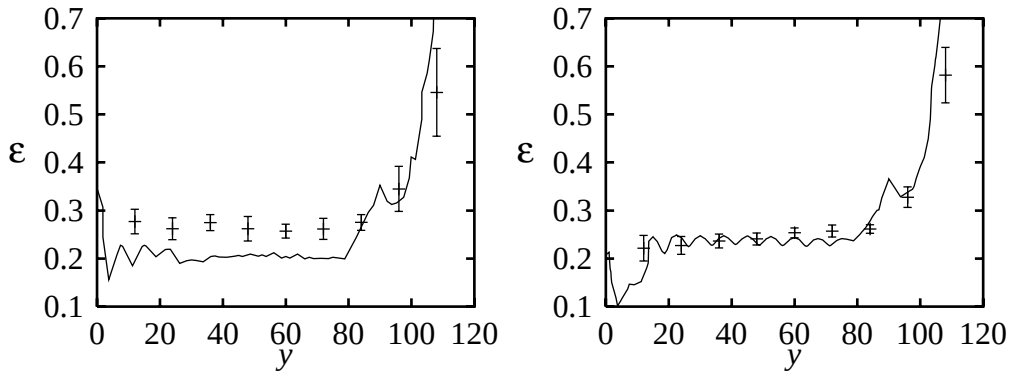

(a) Rib bottom.

(b) Rib flank.

Figure 10: Comparison of experimental and numerical results for gas injection into a plaque with a triangular: residual wall thickness ε as a fraction of the hydraulic radius of the rib triangle (= 4.08 mm) along the axial distance *y* from the gas injection point (error bars = experimental results; solid line = numerical result).

downstream of the gas front (which can be calculated from the Hagen-Poiseuille equation), since that distribution does *not* depend on the constitutive model for the viscosity. Consequently, ε is determined by the flow field at the gas front, which is three-dimensional as advocated in the introduction. One may try to predict this quantity from the two-dimensional Poiseuille flow characteristics of the penetrated liquid downstream of the gas front. However, such attempts are bound to lead to empirical relations (see, *e.g.*, [11, 24, 25]), which may not be generally applicable. For instance, Poslinski *et al.* proposes a relation that has three material-dependent parameters [11]. Those who persist in searching for an empirical relation should realize that the key parameter is the viscosity (or actually: the viscosity distribution), since this is the only parameter left to vary in the Stokes equation that governs the gas penetration problem (equation 6). Nevertheless, as long as a reliable empirical relation is not available, accurate predictions of the gas distribution in GAIM products do require three-dimensional simulations.

5 Conclusions

A three-dimensional model has been developed for the simulation of gas-assisted injection molding processes, and has been implemented in a finite element package. It is based on a physical, rather than on an empirical approach. To avoid elaborate three-dimensional remeshing, a pseudo-concentration method (or: fictitious fluid method) has been adopted, which employs a material label parameter to distinguish the polymer from the gas. It was previously demonstrated that the model is able to qualitatively predict a number of characteristic GAIM phenomena [12].

For the isothermal gas injection experiments, an excellent agreement was found between the experimental and the numerical results, under both Newtonian and shear-thinning

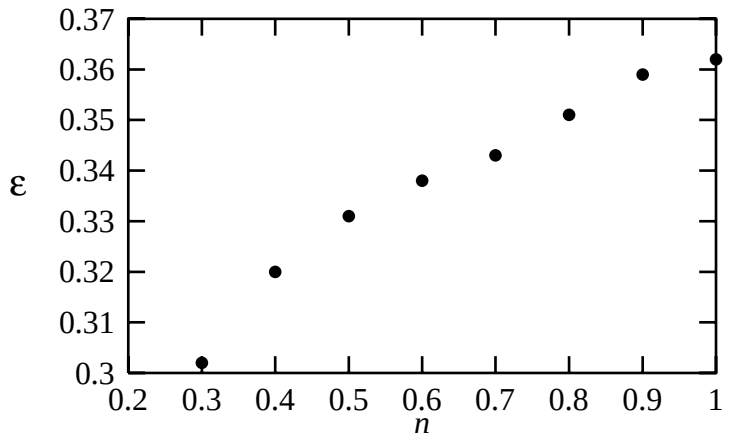

Figure 11: The effect of the power-law exponent n on the residual wall thickness ε for isothermal gas penetration into an axisymmetric cylinder (results from simulations).

conditions. For the non-isothermal case, there was a qualitative agreement in the sense that trend in the residual wall thickness profile was predicted correctly, but the computed residual wall thickness was smaller than the actual experimental value. However, the experimentally obtained residual wall thickness suffered from a particular experimental error, for which a plausible cause has been given.

Due to experimental difficulties, which are related to the sensitivity to instabilities of the gas penetration, only isothermal gas injection experiments were carried out at the plaque-with-rib mold. Once again, the good agreement between experiments and simulations for the plaque-with-rib mold showed, that the model is indeed capable of dealing with a typical, three-dimensional GAIM geometry.

The validation experiments described in Sections 3 and 4 were designed to separate the influences of the parameters that govern the residual wall thickness (most notably shear rate and temperature). For this purpose those experiments served well. It is recommended to further evaluate the computational model by extending the simulations to GAIM under the 'practical' conditions of combined high temperature gradients, high shear rates, and high pressures. In that way, the influence of the process parameters can be studied.

In conclusion, the model that has been developed for gas-assisted injection molding, can predict the final gas distribution in a product and enhance the understanding of the process. In contrast with other models that have been reported in the literature, this model yields the gas penetration from the actual process physics (not from a presupposed gas distribution), is able to deal with the three-dimensional character of the process, incorporates temperature effects and generalized Newtonian viscosity behavior, and has been validated experimentally. As such, this model meets the requirements for successful simulations of industrial gas-assisted injection molding processes.

Once the gas distribution in a GAIM product can be simulated successfully, the next important step will be the prediction of product properties [14]. Since it has been advocated that the reduction of sink marks and of residual stresses are the main advantages of GAIM over conventional injection molding, it will be obvious that these are the product

properties to be focused on. This topic is presently studied in our laboratory.

Acknowledgement

This research was financially supported by the Graduate School Polymer Technology Netherlands.

A Notation

General notation

a, α, A	scalars (regular Latin and Greek symbols)
$\underset{\sim}{a}$	column
A	matrix (upright regular Latin capitals)
a	vector (bold Latin symbols)
A, $\boldsymbol{\alpha}$	second order tensors (bold Latin capitals, bold Greek symbols)

Latin symbols

c	–	material label
c_p	$\mathrm{J\,kg^{-1}\,K^{-1}}$	specific heat capacity
e	$\mathrm{J\,kg^{-1}}$	specific internal energy
e	$\mathrm{m^3}$	computational element volume
h_r	$\mathrm{J\,kg^{-1}}$	reaction heat
H	m	characteristic thickness
L	m	characteristic length
n	–	power-law exponent
p	Pa	pressure
r	$\mathrm{W\,kg^{-1}}$	thermal radiation
R_c	$\mathrm{s^{-1}}$	reaction rate
t	s	time
T	K	temperature
T_g	K	glass transition temperature
$(\Delta T)_0$	K	characteristic temperature difference
U	$\mathrm{m\,s^{-1}}$	characteristic velocity
v	$\mathrm{m^3\,kg^{-1}}$	specific volume

Greek symbols

α	$\mathrm{K^{-1}}$	linear thermal expansion coefficient
ε	–	characteristic height-to-length ratio
ε	–	residual wall thickness ratio
γ	$\mathrm{N\,m^{-1}}$	interfacial tension
Γ		boundary
η	Pa s	shear viscosity

λ	$\mathrm{W\,m^{-1}\,K^{-1}}$	heat conduction coefficient
ϕ	–	cross-sectional liquid fraction; shape function
ρ	$\mathrm{kg\,m^{-3}}$	density
τ	s	characteristic time
ψ	–	(pressure) shape function
Ω		computational domain

Vectors and tensors

$\mathbf{0}$	–	null vector or tensor
$\mathbf{D}$	$\mathrm{s^{-1}}$	rate-of-deformation tensor
$\mathbf{g}$	$\mathrm{m\,s^{-2}}$	gravitational acceleration
$\mathbf{h}$	$\mathrm{W\,m^{-2}}$	heat flux vector
$\mathbf{n}$	m	normal vector
$\mathbf{u}$	$\mathrm{m\,s^{-1}}$	velocity vector
$\mathbf{x}$	m	position vector
σ	Pa	Cauchy stress tensor
τ	Pa	extra stress tensor

Dimensionless numbers

Br	Brinkman number = $\frac{\text{viscous dissipation}}{\text{heat conduction}}$
Ca	Capillary number = $\frac{\text{viscous force}}{\text{interfacial tension force}}$
Fo	Fourier number = $\frac{\text{elapsed time}}{\text{characteristic cooling time}}$
Gc	Gay-Lussac number = (characteristic thermal expansion)$^{-1}$
Pe	Péclet number = $\frac{\text{heat convection}}{\text{heat conduction}}$
Re	Reynolds number = $\frac{\text{inertia force}}{\text{viscous force}}$
Sr	Strouhal number = $\frac{\text{instationary inertia force}}{\text{stationary inertia force}}$

Superscripts

(e)	with respect to a single element
n	at time level n
$*$	dimensionless variable

Subscripts

e	entrance
i (or j)	i^{th} (or j^{th}) component of a column or matrix
n	in normal direction
t	in tangential direction(s)
v	air vent; viscous
w	wall
0	characteristic value; reference value

Operators and functions

$\dot{a}$		material time derivative of a
$\frac{\partial a}{\partial t}$		spatial time derivative of a
Δa		difference in a
∇	m^{-1}	gradient operator
$\lvert a \rvert$		absolute value of a
$\mathbf{A}^d$		deviatoric part of tensor $\mathbf{A}$ ($\mathbf{A}^d = \mathbf{A} - \frac{1}{3}\mathrm{tr}(\mathbf{A})$)
$\mathrm{tr}(\mathbf{A})$		trace (or first invariant) of tensor $\mathbf{A}$
$II_{\mathbf{A}}$		second invariant of tensor $\mathbf{A}$

B Secondary gas penetration in a cylinder

For the cylinder geometry, we can estimate the difference in residual wall thickness between the primary and the secondary gas penetration from the following calculation:

Assume a shrinkage of 5% and a residual wall thickness fraction after primary gas penetration of 0.35. For the cylindrical test sample, R is the (fixed) outer radius, r_1 is the gas channel radius after primary gas penetration, and r_2 is the gas channel radius after secondary gas penetration. For a circular cross-section of a cylindrical sample of length L, the volumes V_1 and V_2 of the polymer material after primary and secondary gas penetration are respectively given by:

$$\begin{aligned} V_1 &= \pi\left(R^2 - r_1^2\right)L \\ V_2 &= \pi\left(R^2 - r_2^2\right)L. \end{aligned}$$

Due to 5% shrinkage, $V_2 = 0.95V_1$, hence:

$$V_2 = \pi\left(R^2 - r_2^2\right)L = 0.95\pi\left(R^2 - r_1^2\right)L.$$

Simple algebraic manipulation yields:

$$r_2 = \sqrt{0.05R^2 + 0.95r_1^2}.$$

Given that $R = 8.5$ mm (see Figure 4), $r_1 = 5.525$ mm and from the above calculation, $r_2 = 5.72$ mm.

Hence, the difference between primary and secondary residual wall thickness is merely 0.2 mm, which is too small to indicate in Figures 5 and 6.

References

[1] K.S. Barton and L.S. Turng, in *ANTEC Proceedings*, 421–425. Society of Plastics Engineers (1994).

[2] C. Rennefeld, Ph.D. thesis, Universität-GH Paderborn (1996), (in German).

[3] L.S. Turng, *Advances in Polymer Technology*, **14**, 1 (1995).

[4] S.Y. Yang and F.Z. Huang, *International Polymer Processing*, **10**, 186 (1995).

[5] P. Eyerer, R. Märtins, and E. Bürkle, *Kunststoffe*, **83**, 505 (1993), (in German).

[6] F. Fairbrother and A.E. Stubbs, *Journal of the Chemical Society*, **1**, 527 (1935).

[7] G.I. Taylor, *Journal of Fluid Mechanics*, **10**, 161 (1961).

[8] B.G. Cox, *Journal of Fluid Mechanics*, **14**, 81 (1962).

[9] B.G. Cox, *Journal of Fluid Mechanics*, **20**, 193 (1964).

[10] W.B. Kolb and R.L. Cerro, *Physics of Fluids A*, **5**, 1549 (1993).

[11] A.J. Poslinski, P.R. Oehler, and V.K. Stokes, *Polymer Engineering and Science*, **35**, 877 (1995).

[12] G.A.A.V. Haagh, H. Zuidema, F.N. van de Vosse, G.W.M. Peters, and H.E.H. Meijer, *International Polymer Processing*, **12**, 207 (1997).

[13] G.A.A.V. Haagh and F.N. van de Vosse, *International Journal for Numerical Methods in Fluids*, **28**, 1355 (1998).

[14] G.A.A.V. Haagh, Ph.D. thesis, Eindhoven University of Technology (1998).

[15] E. Thompson, *International Journal for Numerical Methods in Fluids*, **6**, 749 (1986).

[16] C.W. Hirt and B.D. Nichols, *Journal of Computational Physics*, **39**, 201 (1981).

[17] G.K. Batchelor, An Introduction to Fluid Mechanics, Cambridge University Press, Cambridge etc. (1967).

[18] W.F. Zoetelief, G.W.M. Peters, and H.E.H. Meijer, *International Polymer Processing*, **12**, 216 (1997).

[19] A. Segal, SEPRAN manual, Ingenieursbureau SEPRA, Leidschendam, The Netherlands (1997).

[20] S.Y Yang and F.Z. Huang, in *ANTEC Proceedings*, 747–759. Society of Plastics Engineers (1995).

[21] J.T. Woods, S. Aslam, and J. Birnby, in *ANTEC Proceedings*, 3865–3873. Society of Plastics Engineers (1995).

[22] W.F. Zoetelief, Ph.D. thesis, Eindhoven University of Technology (1995).

[23] H.H. Chiang, C.A. Hieber, and K.K. Wang, *Polymer Engineering and Science*, **31**, 116 (1991).

[24] F. Johannaber, K. Konejung, and R. Plaetschke, *Kunststoffe*, **85**, 763 (1995), (in German).

[25] S.C. Chen and N.T. Cheng, *International Communications in Heat and Mass Transfer*, **23**, 215 (1996).

[26] Dubbel, Dubbel Taschenbuch für den Maschinenbau, Springer, Berlin etc., 18th edn. (1995), (in German).